Volume 11
Number 5
1 May 2026
Pages 983–1176

Reaction Chemistry & Engineering

Linking fundamental chemistry and engineering to create scalable, efficient processes

rsc.li/reaction-engineering

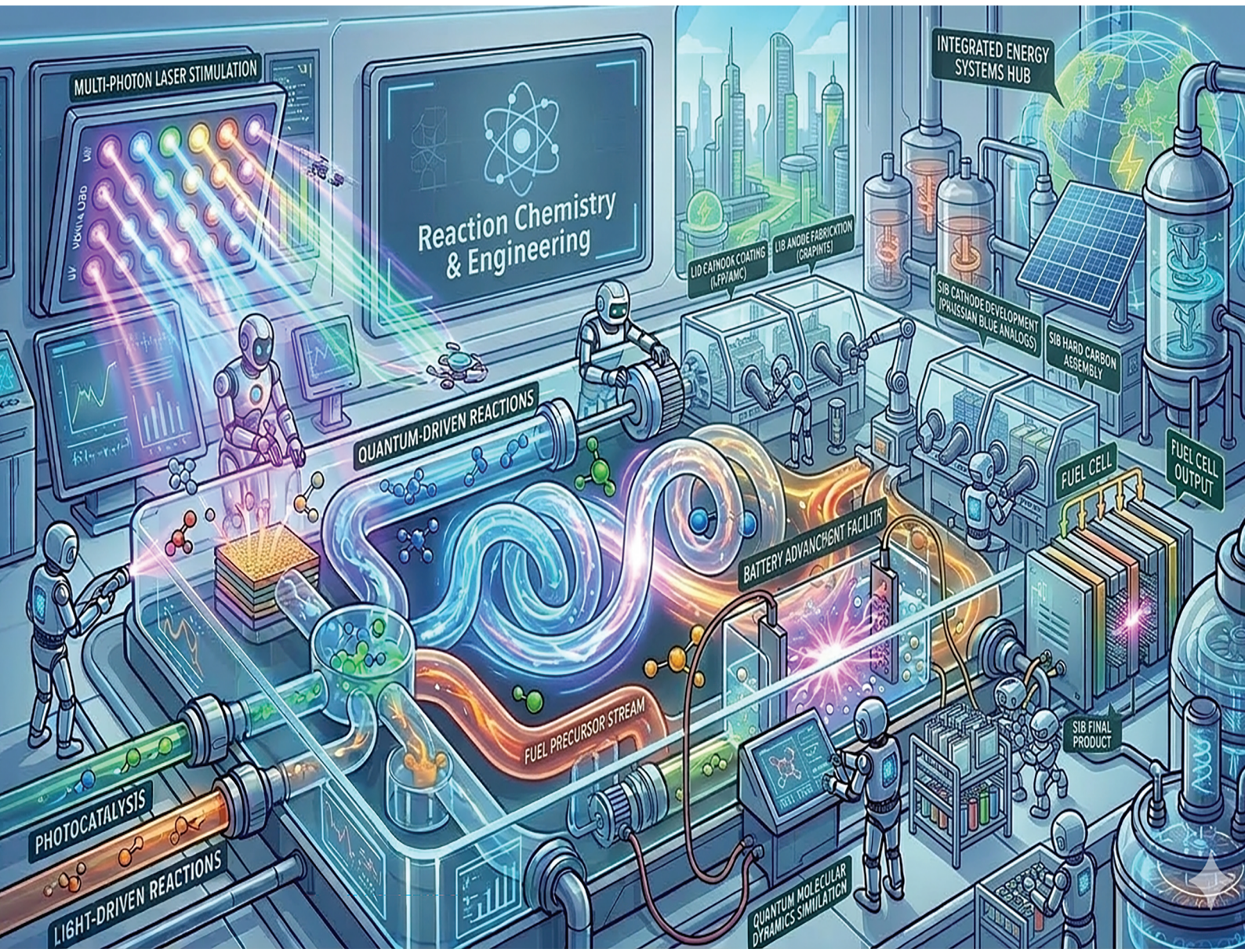

ISSN 2058-9883

ROYAL SOCIETY OF CHEMISTRY

PAPER

Tumelo Seadira *et al.*

Photocatalytic butanol reforming for hydrogen production using Ag_2O/TiO_2 composite catalysts: effects of Ag_2O loading, calcination temperature, and reaction parameters

10 YEARS ANNIVERSARY

Reaction Chemistry & Engineering

ROYAL SOCIETY OF CHEMISTRY

PAPER

View Article Online
View Journal | View Issue

Check for updates

Cite this: *React. Chem. Eng.*, 2026, **11**, 1015

Photocatalytic butanol reforming for hydrogen production using Ag_2O/TiO_2 composite catalysts: effects of Ag_2O loading, calcination temperature, and reaction parameters

Tumelo Seadira, *[a] Thabelo Nelushi,[a] Gullapelli Sadanandam,[b] Dieketseng Tsotesi,[c] Ismaila T. Bello[c] and Mokhotjwa S. Dhlamini[c]

Received 2nd September 2025,
Accepted 17th March 2026

DOI: 10.1039/d5re00384a

rsc.li/reaction-engineering

Over recent years, photocatalytic biomass reforming for hydrogen production has gained research attention as an alternative to the inefficient water-splitting reaction, which requires a standard Gibbs free energy of 237 kJ mol^{-1}. In this study, anatase-phase titanium dioxide (TiO_2) particles were successfully synthesized by employing a sol–gel method, and silver oxide (Ag_2O) nanoparticles with different weight percentages were loaded on the surface of TiO_2 *via* an incipient wet impregnation method to form composite photocatalysts. The structural and optical properties, specific surface areas, and morphology of the photocatalysts were investigated using X-ray diffraction (XRD), UV-vis diffuse reflectance spectroscopy (UV-vis DRS), Brunauer–Emmett–Teller (BET), and scanning electron microscopy (FESEM) analyses. The photocatalytic hydrogen activity of the prepared photocatalysts was studied under visible light irradiation, and it was found that varying the Ag_2O loading influenced this activity. Furthermore, it was found that the calcination temperature and reaction parameters, such as pH and initial butanol concentration, influenced the photocatalytic activity of the prepared photocatalysts for efficient hydrogen production. The highest photocatalytic hydrogen production efficiency was achieved with 0.5 wt% Ag_2O/TiO_2 composite photocatalyst (290 mmol g_{cat}^{-1}). This activity was attributed to 100% anatase crystallite TiO_2 particles that are highly active in terms of the photogeneration of charge carriers; the uniform distribution of Ag_2O on the TiO_2 surface enhanced the suppression of charge-carrier recombination. Finally, the slightly acidic conditions of the butanol mixture facilitated the efficient adsorption of butanol on the surface of the photoexcited photocatalysts, resulting in the simultaneous rapid oxidation of butanol and the efficient production of hydrogen molecules.

1. Introduction

For decades, the world has been highly dependent on non-renewable energy sources, such as fossil fuels, for energy. However, the combustion of fossil fuels emits greenhouse gases, such as carbon dioxide (CO_2), that affect the environment negatively.[1–3] Due to the huge concerns of a shortage of fossil fuels in the next few years from extensive utilization,[4,5] there has been a strong research focus on developing alternative processes for clean energy sources to replace fossil fuels to avoid their negative effects on the environment. Among other alternatives, hydrogen has been promoted as an alternative renewable energy source for the future, which is produced from renewable sources such as biomass and water.[6]

Various commercial methods have been explored to yield hydrogen including steam reforming, pyrolysis, and gasification.[5–7] However, the disadvantages of these methods include the emission of toxic greenhouse gases and the demand for a huge amount of energy, which makes them very expensive. Fujishima and Honda discovered photoelectrochemical water splitting *via* photocatalysis, which paved the way for extended studies in photocatalytic hydrogen production. However, the challenges of water splitting include the requirement for high Gibbs free energy (237 kJ mol^{-1} and 1.23 eV) for separating the hydrogen and oxygen and a backward reaction between both gases.[8] Butanol has been explored for improved photocatalytic reforming and simultaneous efficient hydrogen production due to its high density, low volatility, diminished flammability, and

[a] *Department of Chemical and Materials Engineering, University of South Africa, Johannesburg, 1710, South Africa. E-mail: tumelo.seadira@gmail.com*
[b] *Department of Chemistry, Indira Gandhi National Tribal University, Amarkantak, India*
[c] *Department of Physics, University of South Africa, Johannesburg 1710, South Africa*

hygroscopicity.[9–12] Butanol is a readily made reactant obtainable from renewable sources, by fermentation and other routes.[13–16]

Among other semiconductors used in photocatalysis, TiO_2 is considered one of the most favorable semiconductors, owing to its nontoxicity, low cost, and impressive stability under the reaction conditions.[17] The photocatalytic process on the surface of TiO_2 begins with the generation of charge carriers (e^-/h^+) upon photoexcitation with an energy equal to or greater than the band gap of TiO_2. The excited electrons in the conduction band move to the surface and reduce the pre-adsorbed species, while holes in the valence band are involved in surface oxidation reactions. The photo-excited charge carriers can collapse by recombining on the surface of TiO_2 materials or migrate to the surface, therefore generating split charge carriers, which can engage in the redox reactions occurring on the surface.[18]

Besides TiO_2, the most promising semiconductor used in photocatalysis, bare TiO_2 that results in low activity for sufficient production of hydrogen can be used, mainly because of the large band gap limiting the absorption of light in the UV region, which is only 3–5% in the energy spectrum, and the recombination of the charge carriers.[19–21] To overcome this, metals, non-metals, dyes, and other semiconductors are incorporated on the surface of TiO_2 to reduce the TiO_2 bandgap and enhance the absorption of visible light, thereby enhancing the energy range of photoexcitation and the photocatalytic activity of TiO_2.[2–26] The doping of metal nanoparticles such as Ag_2O into TiO_2 has been reported to enhance the photocatalytic efficiency, which acts as an electron trap, promotes the separation of charge carriers, and therefore delays the recombination of charge carriers.[4,27]

The doping of Ag nanoparticles assists in sensitizing Schottky nanodiodes in the visible light region because of the surface plasmon resonance (SPR) effect[28–30] and facilitates the formation of hot electrons of high kinetic energy under photoirradiation due to the low electron heat capacity of metals, allowing easy and non-adiabatic energy transfer.[29] The incorporation of Ag nanoparticles into TiO_2 with a huge band gap exhibits more efficient stability; however, it displays lower visible light absorption. Therefore, much interest has been focused on developing metal nanoparticle-loaded TiO_2 with various band gaps and surface areas for enhanced photocatalytic hydrogen production activity.[6,21,31–35] To the best of our knowledge, there are limited reports based on the photocatalytic butanol reforming to produce hydrogen. While our prior study[36] systematically investigated the impact of different titania (P25 *vs.* sol–gel) and silver (nitrate *vs.* oxide) precursors on the physicochemical and photocatalytic properties of Ag_2O/TiO_2 composites, the present work focuses on the optimization of a single, well-defined composite system. Specifically, we herein report a detailed study on (i) the effect of Ag_2O loading (0.5–6 wt%) on an anatase TiO_2 matrix, (ii) the critical role of calcination temperature (300–600 °C) on crystallinity and activity, and (iii) the optimization of reaction parameters (pH and butanol concentration) for hydrogen production *via* butanol photoreforming. This comprehensive parametric study provides fundamental insights for designing efficient TiO_2-based photocatalysts for biomass-derived alcohol valorization.

The overall photocatalytic reforming of butanol can be represented by the following reaction:

$$C_4H_9OH + 6H_2O \xrightarrow{h\nu} 4CO_2 + 12H_2,\ \Delta G^\circ > 0.$$

This process involves the oxidation of butanol and the reduction of protons as follows:

$$\text{Oxidation (hole-mediated): } C_4H_9OH + 6H_2O \rightarrow 4CO_2 + 18H^+ + 18e^-,$$

$$\text{Reduction (electron-mediated): } 18H^+ + 18e^- \rightarrow 9H_2.$$

The role of the photocatalyst is to provide photogenerated charges (e^- and h^+) to drive these half-reactions.[37,38]

To the best of our knowledge, there are limited reports based on the photocatalytic butanol reforming to produce hydrogen. However, we have recently published a study on the same topic with a focus on the effects on titania and silver precursors.

Therefore, in this study, we present the preparation of Ag_2O/TiO_2 composite catalysts for photocatalytic hydrogen production *via* butanol reforming under UV-visible light irradiation. More importantly, we present the effect of Ag_2O loading and calcination temperature on the activity of the prepared composite catalysts, as well as the effects of reaction parameters (butanol initial concentration and pH of the solution) on the production of hydrogen. This research describes the utilization of butanol for producing renewable hydrogen, and it can be extended to examine a variety of feedstock such as biomass products.

2. Materials and methods

All reagents were used as received without any additional purification. Butan-1-ol, methanol, P25 (TiO_2), silver nitrate, titanium isopropoxide, and titanium(IV) oxide were sourced from Sigma Aldrich. Sodium phosphate dodecahydrate was obtained from SISCO Research Laboratories. All samples were prepared using ultrapure water from Millipore Direct Q3, supplied by Microsep, South Africa. It is important to note that the methodology used in this study was adapted from our recently published work;[36] however, this study explores different specific objectives compared to the previously published paper.

2.1. Preparation of TiO_2 nanoparticles and AgO_2/TiO_2 composites

Pure TiO_2 nanoparticles were prepared by a sol–gel method.[36,39] Titanium isopropoxide (TTIP) was used as the titania precursor. The molar ratios of titanium isopropoxide (50 mL), methanol, and deionized water were set at 1 : 1 : 65. The liquid resultant

was obtained by mixing TTIP with methanol, followed by sonication for 5 min. To the solution, distilled water was added dropwise, while the mixture was stirred vigorously in a beaker under reflux conditions at 80 °C for 3 h. The remaining liquid mixture was allowed to cool, filtered using a centrifuge, and then washed twice with methanol. The final product was dried at 80 °C for 12 hours and subsequently calcined at 450 °C for 3 hours. An incipient wet impregnation method was employed to load different amounts of Ag_2O (ranging from 0.5% to 6% by weight) onto the surface of TiO_2 particles. The prepared composites were dried at 80 °C overnight and then calcined at 450 °C for 3 hours. The catalysts containing 0.5%, 1%, 2%, 3%, 4%, 5%, and 6% Ag_2O loaded onto TiO_2 are labeled as 0.5 wt% Ag_2O/TiO_2, 1 wt% Ag_2O/TiO_2, 2 wt% Ag_2O/TiO_2, 3 wt% Ag_2O/TiO_2, 4 wt% Ag_2O/TiO_2, 5 wt% Ag_2O/TiO_2, and 6 wt% Ag_2O/TiO_2. Additionally, the 0.5 wt% Ag_2O/TiO_2 photocatalyst was further calcined at 300 °C, 400 °C, 500 °C, and 600 °C for 3 hours.

2.2. Characterization

The crystal structures of the samples were recorded using an X-ray diffractometer (Rigaku SmartLab) with Cu-Kα radiation (λ = 0.15405 nm), operating at a current of 200 mA and 45 kV. The BET (Brunauer–Emmett–Teller) surface areas and porosity properties of the photocatalysts were obtained using the Autosorb-I (Quantachrome) equipment through N_2 adsorption at −196 °C. Before this analysis, the samples were degassed at 150 °C for 24 hours. Additionally, the UV-vis diffuse reflectance spectra were recorded using a Lambda 750S UV-vis spectrophotometer over a wavelength range of 200–800 nm. The band gap of the semiconductor was determined using a Tauc plot. To analyze the morphologies and chemical compositions of the samples, a scanning electron microscope (SEM-EDS JEOL JSM-7800F) equipped with an EDS detector was utilized.

2.3. Photocatalytic activity testing procedure

The visible light-driven photocatalytic butanol reforming for hydrogen production activity tests was carried out using a solar simulator (HAL3200 compact xenon lamp light source). The prepared composite photocatalyst, together with the butanol solution and a magnetic stirrer bar, was added to a 50 mL quartz reactor, which was enclosed with a silicone rubber septum to prevent the escape of generated gas. The helium gas was then bubbled in the mixture for 30 minutes to purge the dissolved oxygen and air to create an anaerobic environment in the reactor. The reactor was then placed on the magnetic stirrer to keep the composite photocatalyst in suspension, and the reactor was subjected to photoirradiation using a solar simulator. A syringe (Gerstel) was used to extract 0.5 mL sample of the evolved gas at an hour interval for four hours from the quartz reactor through the silicone rubber septum; and the gas sample was subsequently injected into the GC (Shimadzu GC-2010) fitted with a Stabilwax column and a BID detector, using helium as a gas carrier, to quantify the generated hydrogen from butanol reforming. The GC was first calibrated using a five-point calibration method by GC until a calibration curve with R = 0.999 was achieved. Thereafter, a 0.5 mL sample of gas was extracted from the photocatalytic reactor and injected into the GC to determine the hydrogen concentration.[36]

3. Results and discussion

3.1. SEM analysis

Fig. 1(a and b) displays the SEM images of bare nano TiO_2 and 0.5 wt% Ag_2O/TiO_2 samples, all of which were calcined at 450 °C. No significant differences in surface morphology were observed among the samples. Each sample exhibited a spherical morphology, with dense structures distributed uniformly throughout. Energy-dispersive X-ray (EDX) analysis was conducted to detect the presence of silver (Ag) on the surface of TiO_2 nanoparticles. Fig. 1(c) illustrates the peaks for titanium (Ti) and oxygen (O), and Fig. 1(d) shows similar peaks plus a silver (Ag) peak in the optimized 0.5 wt% Ag_2O/TiO_2 sample, confirming the presence of Ag within the TiO_2 nanoparticles. The small peaks in the analysis can be attributed to the low concentrations of Ag dopants on the surface of TiO_2. The observed carbon peaks are attributed to the carbon coating applied to minimize the charging effects during SEM-EDX analysis, whereas the oxygen peak is ascribed to residual oxygen introduced during the sample preparation process, which involved the use of water.

3.2. XRD analysis

Fig. 2 shows the XRD patterns of bare nano TiO_2 and Ag_2O/TiO_2 composite samples with different Ag loadings, which were calcined at 450 °C. All samples show sharper diffraction peaks, which are evidence of the crystallinity of the samples that can be readily indexed for their heterostructures. The photocatalysts visibly exhibit the characteristic planes of the anatase phase by a series of strong peaks at 2θ = 25.3° (101), 37.8° (004), 48.0° (200), and 62.6° (204) (JCPSD, No. 21-1272).[20,41,42] No distinct diffraction peaks corresponding to crystalline Ag_2O phases were detected, which may be attributed to its high dispersion, low crystallinity, or small particle size below the XRD detection limit.[40]

3.3. N_2 adsorption/desorption isotherms

To investigate the surface area properties and pore size distribution of the photocatalysts, we performed a nitrogen (N_2) adsorption–desorption analysis using the BJH method. Fig. 3 shows the N_2 adsorption–desorption isotherms for the catalysts, which display type IV (a) isotherms and H2 (b)-shaped hysteresis loops for both bare nano TiO_2 and 0.5 wt% Ag_2O/TiO_2, according to the IUPAC classification.[41,42] Notably, the 0.5 wt% Ag_2O/TiO_2 sample demonstrated an H3 hysteresis loop. All photocatalysts exhibited mesopore characteristics, evidenced by the type IV (a) isotherms.[42] The presence of a small hysteresis loop may indicate that the Ag oxide particles are blocking pore channels and/or degrading

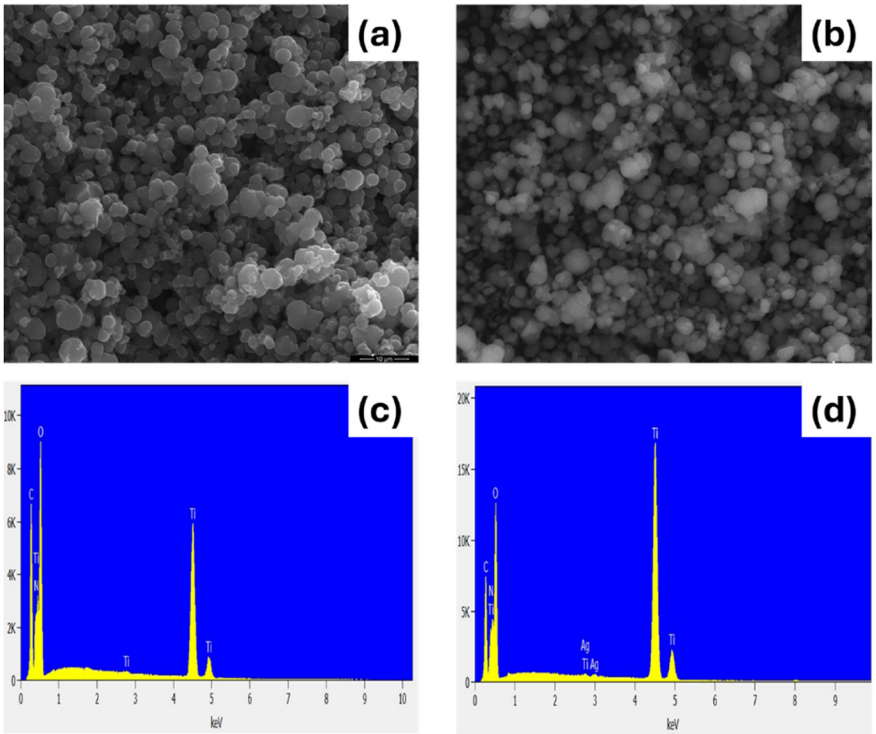

Fig. 1 SEM images of (a) bare TiO_2 and (b) 0.5 wt% Ag_2O/TiO_2. EDS analysis plots of (c) bare TiO_2 and (d) 0.5 wt% Ag_2O/TiO_2.

the TiO_2 heterostructure. The BJH pore size distribution plots in Fig. 4 reveal a narrow distribution, indicating homogeneity in pore sizes. Table 1 summarizes the BET specific surface areas, pore volumes, and particle sizes for the bare nano TiO_2 sample and the Ag_2O/TiO_2 samples. The BET results showed that the bare nano TiO_2 sample has a high surface area of 218 $m^2\ g^{-1}$, which can be attributed to its nanoparticle size.[25,38] In contrast, the Ag_2O/TiO_2 samples exhibited decreased surface areas ranging from 209 to 29 $m^2\ g^{-1}$, likely due to pore blockage in TiO_2 caused by the deposition of Ag oxide.[43–45]

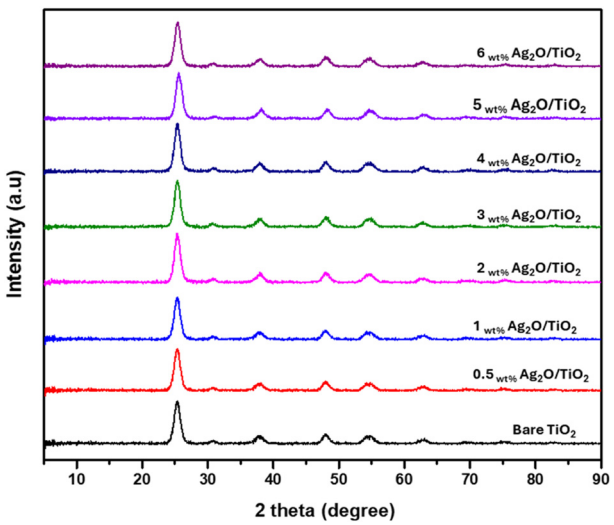

Fig. 2 X-ray diffraction patterns of the bare TiO_2 and Ag_2O/TiO_2 samples with different Ag loadings, which were calcined at 450 °C.

3.4. UV-visible diffuse reflectance spectroscopy (UV-vis DRS)

The diffuse reflectance spectroscopy (DRS) technique was used to identify the optical properties of the prepared photocatalysts. Fig. 5a shows the DRS spectra of bare nano TiO_2 and Ag_2O/TiO_2 samples with different Ag_2O loadings. Bare nano TiO_2 shows an absorption edge of approximately 398 nm due to the charge transfer from the valence band to the conduction band.[46] The absorption spectrum of Ag_2O/TiO_2 samples shifted further to the visible light spectrum (400–500 nm), which is attributed to Ag_2O loaded onto the TiO_2 surface. It was observed that the absorption edge shifted further to the visible range with the increase in Ag_2O loading. The loading of Ag metal onto the TiO_2 surface causes impurity, thereby narrowing the band gap between the conduction and valence bands.[46] The shift of the absorption edge to longer wavelengths for Ag_2O loaded onto nano TiO_2 indicates excellent interaction between the TiO_2 and Ag particles, thereby improving the photocatalytic activity of the catalysts in the visible light. This shifts the band edge into the visible region due to the red shift.[47]

The energy band gaps of the photocatalysts were determined from the UV-vis spectra using the Tauc plots, as shown in Fig. 5b. The energy band gap of bare nano TiO_2 was measured to be 3.16 eV. In contrast, a decrease in the energy band gap of the Ag_2O/TiO_2 catalysts, ranging from 3.13 eV to 2.9 eV, was observed. This reduction is attributed

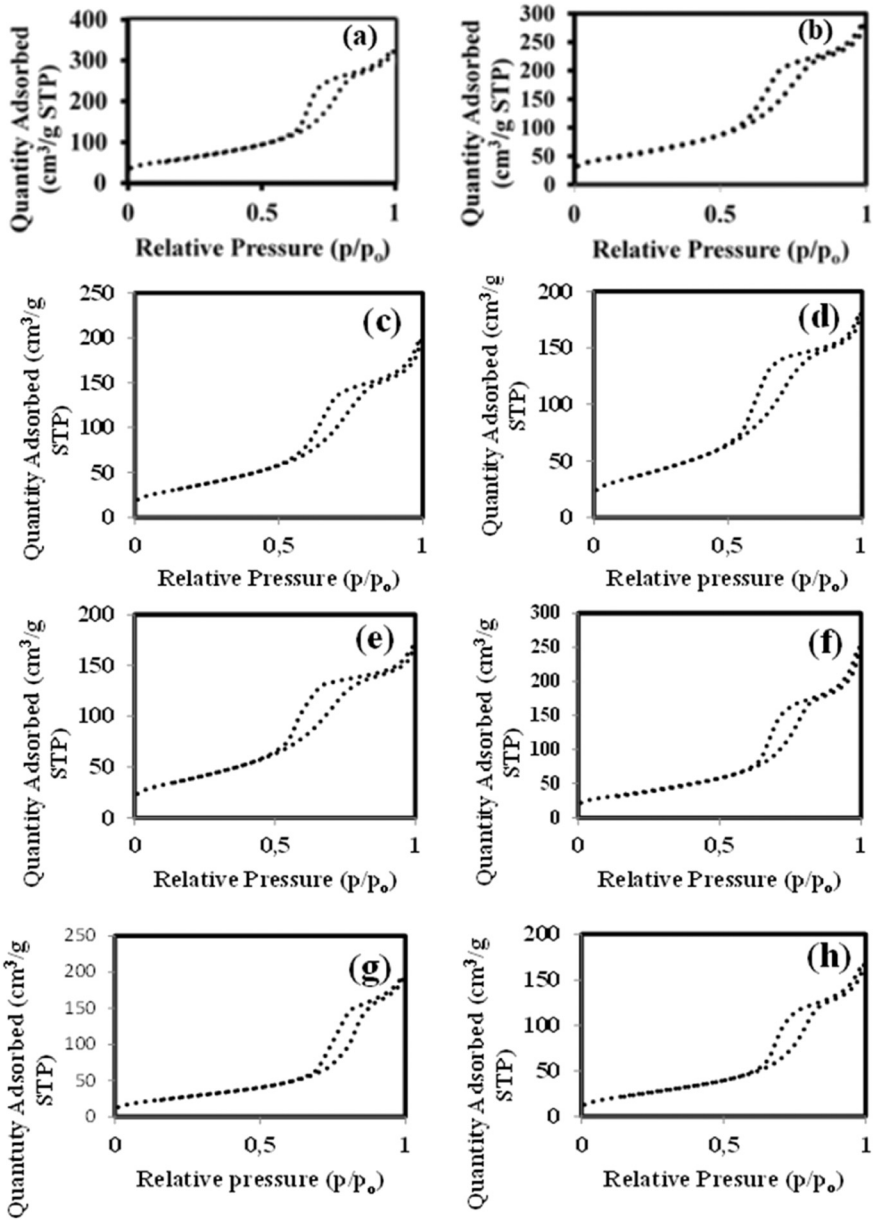

Fig. 3 Nitrogen adsorption–desorption isotherms of (a) bare TiO_2; (b) 0.5 wt% Ag_2O/TiO_2; (c) 1 wt% Ag_2O/TiO_2; (d) 2 wt% Ag_2O/TiO_2; (e) 3 wt% Ag_2O/TiO_2; (f) 4 wt% Ag_2O/TiO_2; (g) 5 wt% Ag_2O/TiO_2 and (h) 6 wt% Ag_2O/TiO_2.

to the incorporation of silver (Ag) metal onto the surface of TiO_2.[48]

4. Photocatalytic H_2 evolution activity

The studies on photocatalytic hydrogen production were conducted over Ag_2O/TiO_2 catalysts calcined at 450 °C, fixed at 1% (v/v) butanol : water mixtures under UV-vis light. Fig. 6 shows the effect of Ag_2O loading on the photocatalytic hydrogen production activity of the prepared samples. The rate of hydrogen production rapidly increased from 16 mmol $g_{catalyst}^{-1}$ to 255 mmol $g_{catalyst}^{-1}$ with 0.5 wt% Ag_2O. However, the rate of hydrogen production decreases with the increase in Ag_2O loading. The high activity of 0.5 wt% could be attributed to the high surface area that traps more sacrificial butanol molecules into the active site of TiO_2 and the reduced band gap (3.13 eV), which enhance butanol reforming and the successive reduction of H^+ into H_2.[49] The lower rate of hydrogen production with a higher metal loading could be attributed to aggregation and metal dispersion, allowing them to serve as recombination centers for charge carriers.[50] This was also confirmed by the photoluminescence analysis of TiO_2 composites with different metal loadings reported in our previously published work.[40] We demonstrated that with the low loading of the metal nanoparticles on the surface of TiO_2, the metal nanoparticles trap the photoinduced electrons, thereby suppressing the electron/hole pair recombination rate on TiO_2. Furthermore, this suppression of the electron/hole recombination rate allows

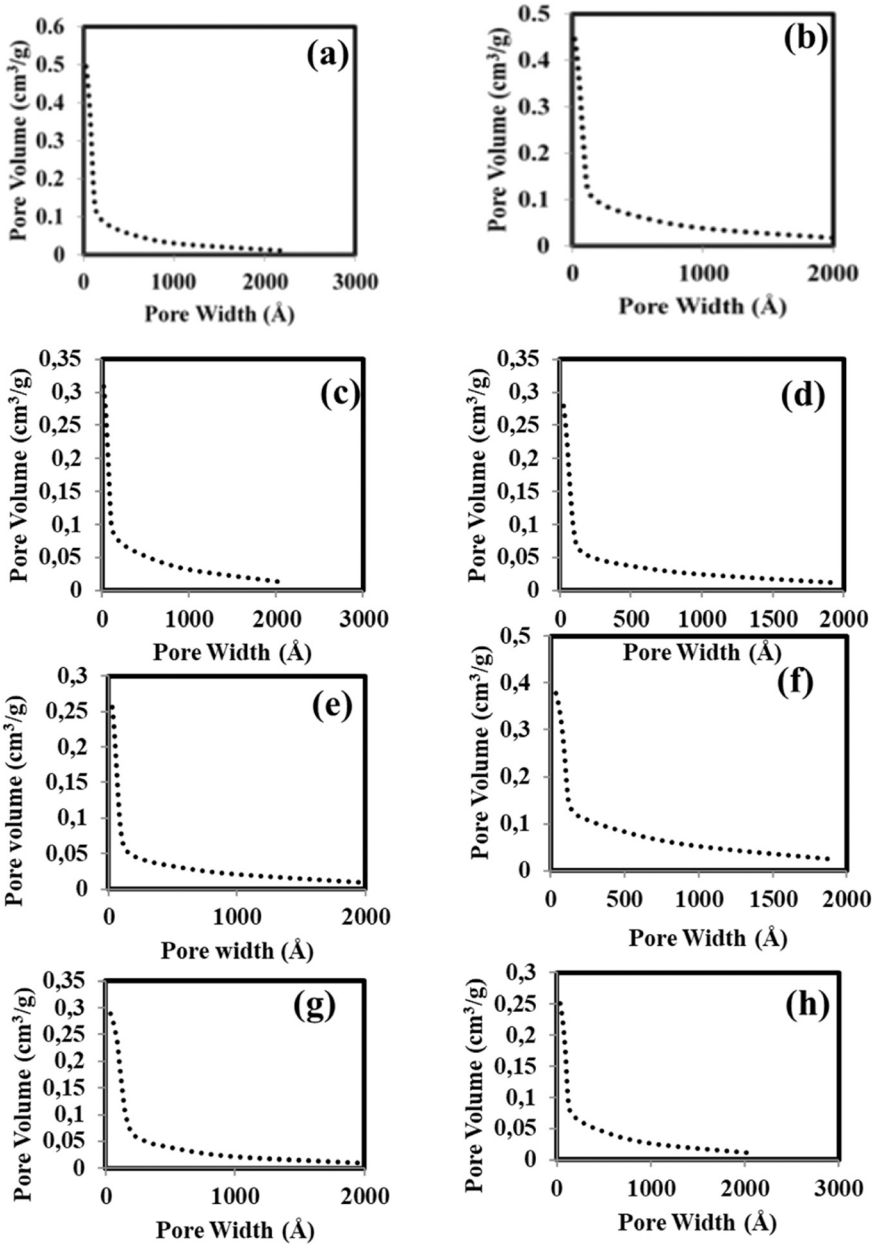

Fig. 4 BJH pore size distribution plots of (a) bare TiO_2; (b) 0.5 wt% Ag_2O/TiO_2; (c) 1 wt% Ag_2O/TiO_2; (d) 2 wt% Ag_2O/TiO_2; (e) 3 wt% Ag_2O/TiO_2; (f) 4 wt% Ag_2O/TiO_2; (g) 5 wt% Ag_2O/TiO_2 and (h) 6 wt% Ag_2O/TiO_2.

Table 1 Physical characteristics of the prepared Ag_2O/TiO_2 materials

Catalysts	Calcination temperature (°C)	BET surface area ($m^2\ g^{-1}$)	Pore volume ($cm^3\ g^{-1}$)	Nanoparticle size (nm)
Bare nano TiO_2	450	218	0.49	27.56
0.5 wt% Ag_2O/TiO_2	450	199	0.43	30.21
1 wt% Ag_2O/TiO_2	450	130	0.30	46.00
2 wt% Ag_2O/TiO_2	450	144	0.27	41.63
3 wt% Ag_2O/TiO_2	450	141	0.25	42.69
4 wt% Ag_2O/TiO_2	450	134	0.36	44.77
5 wt% Ag_2O/TiO_2	450	97	0.29	61.75
6 wt% Ag_2O/TiO_2	450	94	0.25	64.13

the oxidation of the sacrificial agent, such as butanol, efficiently for rapid production of H^+, and subsequently, enhances the production of hydrogen molecules.[40] The hydrogen yield peaks at 0.5 wt% Ag_2O loading (255 mmol g^{-1}) and then decreases.

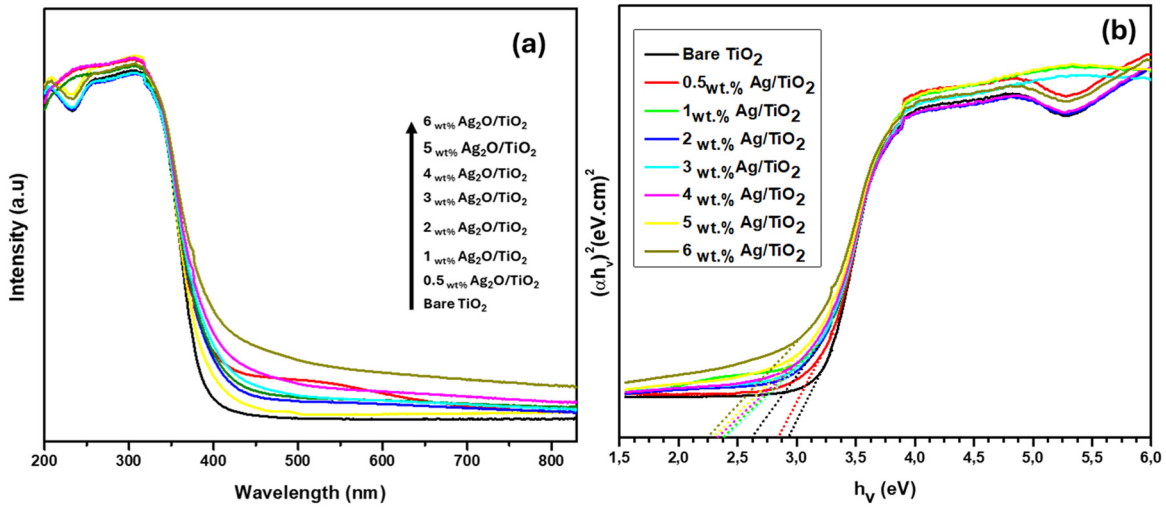

Fig. 5 (a) DRS spectra and (b) Tauc plots of the prepared Ag_2O/TiO_2 materials.

The non-linear decline between 1 and 4 wt% likely reflects a complex interplay where the detrimental effect of decreasing surface area (Table 1) is partially offset by increased visible light absorption (Fig. 5a). However, beyond 4 wt%, severe pore blockage/aggregation (Table 1) and the dominance of Ag species as recombination centers lead to a pronounced activity decrease.

4.1. Effects of calcination temperature

Fig. 7 shows the hydrogen production activity studies of 0.5 wt% Ag_2O/TiO_2 with different calcination temperatures at 5% concentration of butanol solution under UV-visible light. The photocatalysts were calcined at 300 °C, 400 °C, 450 °C, 500 °C, and 600 °C. High hydrogen production activity of 289 mmol $g_{catalyst}^{-1}$ was achieved using 450 °C calcination temperature. Low photocatalytic activity is attributed to low surface area. The 0.5 wt% Ag_2O/TiO_2 sample was concluded to be a highly active catalyst and used for further studies. The characterization of the effect of calcination temperature can be found in the supplementary material. The highly active catalyst was further confirmed by BET results provided in Table S1, which attributes the enhanced activity to the high surface area of the catalyst as well as the complete anatase phase of the composite material.[51]

4.2. Effects of reaction parameters

The photocatalytic performance for hydrogen production activity was tested to study the effect of the initial pH of the butanol solution under UV-vis light. The influence of pH was studied. Fig. 8 shows the pH of the butanol solutions.[52] The highest activity was observed at a pH of 5.5 (290 mmol $g_{catalyst}^{-1}$), attributed to the more positive H^+/H_2 redox potential, which resulted in efficient hydrogen photocatalytic generation.[53] Furthermore, this enhanced activity at pH 5.2

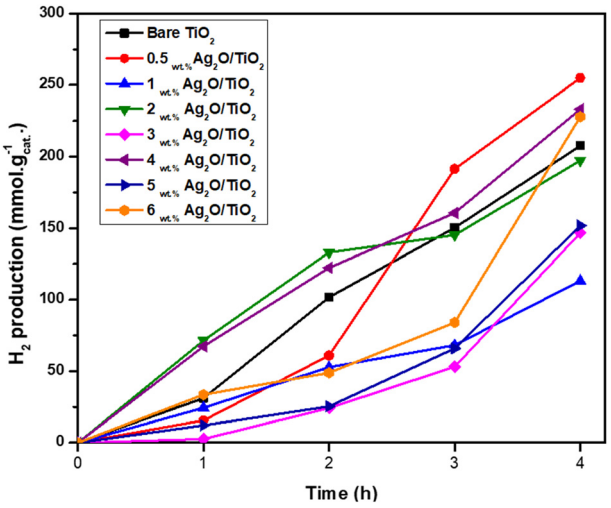

Fig. 6 Photocatalytic production of hydrogen from butanol reforming using the prepared Ag_2O/TiO_2 materials.

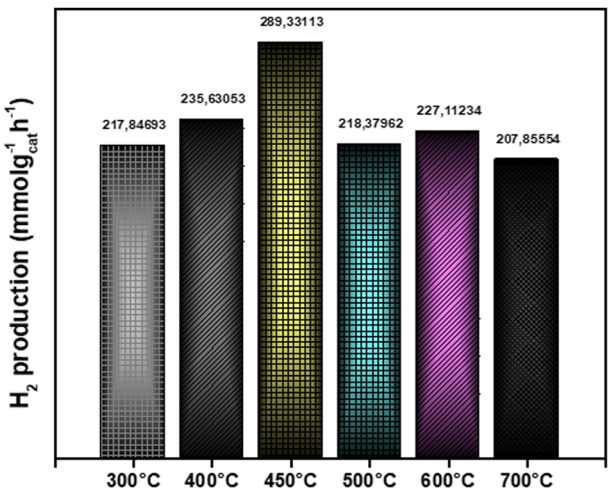

Fig. 7 Photocatalytic hydrogen production activity over 0.5 wt% Ag_2O/TiO_2: effect of different calcination temperatures.

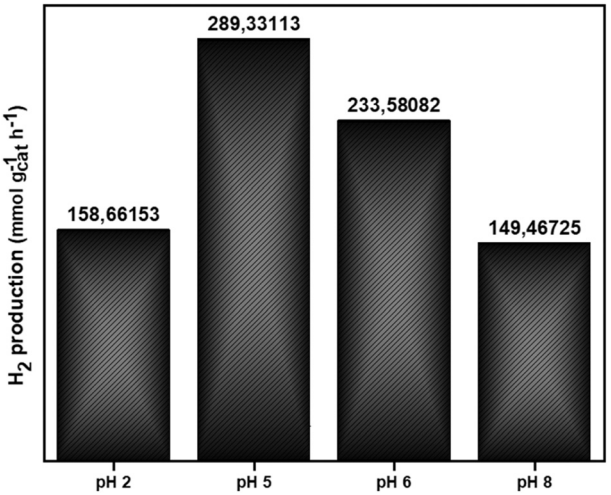

Fig. 8 Photocatalytic hydrogen production activity over 0.5 wt% Ag_2O/TiO_2 catalyst: effect of different pH values of the butanol solution.

can be attributed to the interplay between surface charge (PZC of $TiO_2 \approx 6.2$) and butanol adsorption.[54]

Fig. 9 shows the rate of hydrogen production with different initial butanol concentrations over 0.5 wt% Ag_2O/TiO_2 catalysts calcined at 450 °C. An increase in the concentration of butanol resulted in a significant increase in hydrogen production. A rapid increase was observed with 5% (v/v) butanol concentration. Furthermore, the figure shows a clear increase up to 5% (v/v) butanol, followed by saturation, indicative of active site limitation at high concentrations.[40] The hydroxylic absorption sites become saturated as the reactant concentration increases. The production of a respective number of reactive species on the surface of the catalyst does not increase, which could be due to the constant light intensity and the amount of catalyst.[55,56] Nonetheless, at a higher concentration, the reaction at the interface influences the entire process owing to the adsorption saturation of butanol on the catalyst surface.

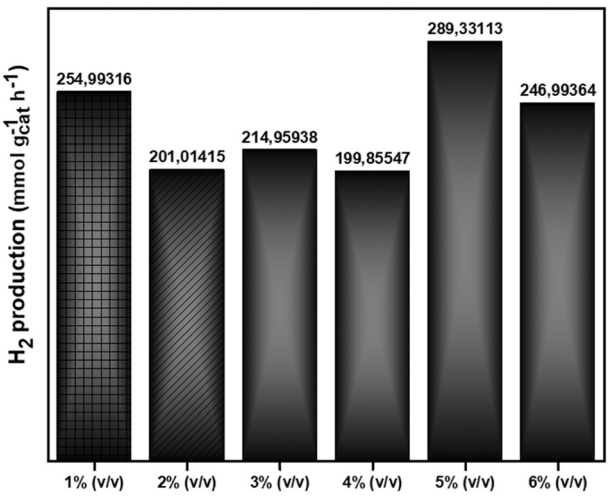

Fig. 9 Photocatalytic hydrogen production activity over 0.5 wt% Ag_2O/TiO_2: effect of different initial butanol concentrations in % (v/v).

5. Conclusions

In summary, Ag_2O/TiO_2 composite catalysts with different Ag_2O loadings were successfully prepared using both the sol–gel method and the incipient wet impregnation method. It was observed that incorporating Ag nanoparticles onto the surface of anatase TiO_2 enhanced the photocatalytic activity of the composite catalyst by suppressing the recombination of electron–hole pairs. However, the photocatalytic activity tended to decrease as the Ag loading increased. This decline is attributed to the Ag nanoparticles inhibiting the efficient excitation of the surface of TiO_2 by light photons, acting as recombination centers. The highest photocatalytic activity of the Ag_2O composite catalysts was achieved with 0.5 wt% Ag loading. Additionally, it was demonstrated that the calcination temperature is crucial in catalyst preparation. The activity of the composite catalyst increased with higher calcination temperatures, up to 450 °C, after which it decreased.

Above 450 °C, the composite catalyst begins to develop the rutile phase, which is less active than the anatase phase. Reaction parameters such as the initial concentration of butanol and its pH play a crucial role in the photocatalytic hydrogen production process. The hydrogen production activity of the composite catalyst depends on how the pH affects the surface charge of both the catalyst and the butanol solution. The maximum rate of hydrogen production occurs when the pH of the butanol solution is slightly acidic (pH 5.5). This is because the surface charge of the TiO_2 particles is nearly neutral, allowing for the efficient adsorption and oxidation of butanol molecules and, consequently, the reduction of H^+ ions to hydrogen molecules. Furthermore, an increase in butanol concentration leads to a slight increase in hydrogen evolution; however, this effect levels off when the concentration exceeds 5% (v/v). This study has opened new frontiers for further research into enhancing TiO_2-based photocatalysts for hydrogen production through butanol reforming. While the observed red-shift in DRS and enhanced activity strongly suggest improved charge separation, direct spectroscopic evidence (*e.g.*, photoluminescence and transient absorption) of reduced recombination kinetics would further solidify the proposed mechanism, which is recommended for future work. The proposed and detailed photocatalytic butanol reforming for photocatalytic hydrogen production is reported in our previously published work.[36]

Author contributions

Tumelo Seadira: conceptualization, data curation, formal analysis, funding acquisition, investigation, supervision, methodology, validation, writing – original draft, and writing – review and editing. Thabelo Nelushi: conceptualization, data curation, formal analysis, funding acquisition, investigation,

methodology, validation, writing – original draft, and writing – review and editing. Gullapelli Sadanandam: conceptualization, data curation, formal analysis, funding acquisition, investigation, supervision, methodology, validation, writing – original draft, and writing – review and editing. Ismaila T. Bello: conceptualization, data curation, formal analysis, funding acquisition, investigation, supervision, methodology, validation, writing – original draft, and writing – review and editing. Dieketseng Tsotetsi: conceptualization, data curation, formal analysis, funding acquisition, investigation, supervision, methodology, validation, writing – original draft, and writing – review and editing. Mokhotjwa S. Dhlamini: conceptualization, data curation, formal analysis, funding acquisition, investigation, supervision, methodology, validation, writing – original draft, and writing – review and editing.

Conflicts of interest

The authors declare no conflicts of interest.

Data availability

Supplementary information (SI) is available. See DOI: https://doi.org/10.1039/d5re00384a.

Acknowledgements

The authors would like to acknowledge that this work has been supported in part by the University of South Africa (Unisa) and the National Research Foundation (NRF) of South Africa. The authors also extend their gratitude to the Indira Gandhi National Tribal University (IGNTU) for their support in encouraging the research. The opinions, findings, and conclusions/recommendations expressed in this publication are those of the authors, and the NRF accepts no liability whatsoever in this regard.

References

1 N. M. Ngo, M. D. Nguyen, H. V. Tran, R. Medhi, J. M. Lee and T. R. Lee, Photocatalytic Hydrogen Generation by Monodisperse TiO2 Nanoparticles Singly and Dually Doped with Niobium and Tantalum, *ACS Appl. Nano Mater.*, 2025, **8**(9), 4841–4851, DOI: 10.1021/acsanm.5c00391.

2 A. Gutiérrez, D. Ramírez-Ortega, B. Portales and R. Zanella, Enhanced photocatalytic hydrogen production on Au/TiO2-CeO2 through the formation of oxygen vacancies, *Mater. Sci. Semicond. Process.*, 2025, **197**, 109703, DOI: 10.1016/j.mssp.2025.109703.

3 O. F. Aldosari, Photocatalytic water-splitting for hydrogen production using TiO2-based catalysts: Advances, current challenges, and future perspectives, *Catal. Rev.*, 2025, 1–38, DOI: 10.1080/01614940.2024.2446476.

4 A. K. Wahab and H. Idriss, Study of the photocatalytic reforming and oxidation of Glycerol over Ag–Pd/TiO2, *Int. J. Hydrogen Energy*, 2024, **52**, 159–171, DOI: 10.1016/j.ijhydene.2023.05.344.

5 A. N. Tuama, *et al.*, Electron donors' approach to enhance photocatalytic hydrogen production of TiO_2: a critical review, *Transition Met. Chem.*, 2025, **50**, 863–882, DOI: 10.1007/s11243-025-00663-5.

6 M. Umair, *et al.*, Pt-Nb2O5-TiO2 based semiconductors for photo-reforming of glucose and fructose aqueous solutions, *Appl. Surf. Sci.*, 2024, **648**, 159030, DOI: 10.1016/j.apsusc.2023.159030.

7 M. Umair, *et al.*, Biomass derivatives photoreforming in pilot plant scale to obtain H2 under green conditions by using ball milling Cu2O-TiO2 P25 photocatalysts, *Chem. Eng. J.*, 2025, **504**, 158585, DOI: 10.1016/j.cej.2024.158585.

8 Z. X. Huang, *et al.*, Defect Engineering of Ultrasmall TiO2 Nanoparticles Enables Highly Efficient Photocatalysts for Solar H2 Production from Woody Biomass, *Nano Lett.*, 2024, **24**(38), 11968–11975, DOI: 10.1021/acs.nanolett.4c03361.

9 Y. Guo, *et al.*, Steam reforming of n-butanol and tetrahydrofuran: Influence of aliphatic carbon chain and furan ring on coking behaviors, *Int. J. Hydrogen Energy*, 2024, **50**, 715–725, DOI: 10.1016/j.ijhydene.2023.11.145.

10 A. R. Q. Gonçalves, J. P. da S. Q. Menezes, R. L. Manfro and M. M. V. M. Souza, Hydrogen Production by Steam Reforming of Acetone–Butanol–Ethanol over Supported Nickel Catalysts: Effect of MgO Promoter, *ACS Omega*, 2025, **10**(37), 43053–43060, DOI: 10.1021/acsomega.5c06102.

11 C. Suppaso, C. Khamdang, S. Suthirakun, K. Maeda and N. Khaorapapong, Photocatalytic hydrogen production from butanol-water mixture over noble-metal free CuO/NiO/NiFe2O4 heterostructure, *Int. J. Hydrogen Energy*, 2025, **97**, 994–1001, DOI: 10.1016/j.ijhydene.2024.11.390.

12 J. Li, Y. Zhang, K. Sun, W. Liu, H. Yan and J. Meng, Optimization of a cathodic electro-fermentation process for enhancing co-production of butanol and hydrogen via acetone-butanol-ethanol fermentation of Clostridium beijerinckii, *Energy Convers. Manage.*, 2022, **251**, 114987, DOI: 10.1016/j.enconman.2021.114987.

13 K. Kumar, S. M. Jadhav and V. S. Moholkar, Acetone-Butanol-Ethanol (ABE) fermentation with clostridial co-cultures for enhanced biobutanol production, *Process Saf. Environ. Prot.*, 2024, **185**, 277–285, DOI: 10.1016/j.psep.2024.03.027.

14 G. Du, Y. Wu, W. Kang, Y. Xu, S. Li and C. Xue, Enhanced butanol production in Clostridium acetobutylicum by manipulating metabolic pathway genes, *Process Biochem.*, 2022, **114**, 134–138, DOI: 10.1016/j.procbio.2022.01.021.

15 Y. Guo, *et al.*, Production of butanol from lignocellulosic biomass: recent advances, challenges, and prospects, *RSC Adv.*, 2022, **12**(29), 18848–18863, DOI: 10.1039/D1RA09396G.

16 S. Riaz, *et al.*, Biobutanol production from sustainable biomass process of anaerobic ABE fermentation for industrial applications, *Arch. Microbiol.*, 2022, **204**, 672, DOI: 10.1007/s00203-022-03284-z.

17 M. Umair, *et al.*, Investigating the activity of modified TiO2 photocatalysts used for the photoreforming of biomass derivatives, *J. Photochem. Photobiol., A*, 2024, **453**, 115654, DOI: 10.1016/j.jphotochem.2024.115654.

18 E. M. N. T. Edirisooriya, P. S. Senanayake, P. Xu, M. R. Talipov and H. Wang, Optimization of green hydrogen evolution from low-density plastics using TiO2-based nano-photocatalysts with techno-economic and carbon footprint assessment, *Nanotechnol. Environ. Eng.*, 2024, **9**(4), 817–832, DOI: 10.1007/s41204-024-00397-2.

19 A. D. G. Kafadi, *et al.*, Recent Trends in Hydrogen Generation Using TiO_2-Based Photocatalyst via Photocatalytic Water Splitting, *Eur. J. Inorg. Chem.*, 2025, **28**, e202500191, DOI: 10.1002/ejic.202500191.

20 A. Khan, *et al.*, Cu-Based MOF/TiO2 Composite Nanomaterials for Photocatalytic Hydrogen Generation and the Role of Copper, *Adv. Funct. Mater.*, 2025, 2501736, DOI: 10.1002/adfm.202501736.

21 A. Diego-Lopez, L. Tamarit, M. L. Marin and F. Bosca, Boosting TiO2 photocatalytic hydrogen production via silica-core engineering, optimized shell architecture, and Pd nanoparticles decoration, *Chem. Eng. J.*, 2026, **532**, 174350, DOI: 10.1016/j.cej.2026.174350.

22 R. Ma, G. Williams, M. Muscetta and S. Vernuccio, Enhanced photocatalytic hydrogen evolution via ball-milled PtO2/TiO2 heterojunction photocatalyst: An alternative approach for efficient energy production, *Chem. Eng. J.*, 2025, **507**, 160228, DOI: 10.1016/j.cej.2025.160228.

23 T. Kanwal, *et al.*, Solar driven photocatalytic glycerol and glucose reforming via noble metals free BiOX (X = Cl, Br, I)-TiO2 composites, *Sustainable Mater. Technol.*, 2026, **47**, e01825, DOI: 10.1016/j.susmat.2025.e01825.

24 Y. Wang, *et al.*, Enhanced photocatalytic H2 evolution from glucose reforming on CuNi-decorated oxygen-vacancy-rich black TiO2 nanosheets, *Fuel*, 2026, **408**, 137665, DOI: 10.1016/j.fuel.2025.137665.

25 A. Meng, R. Yang, W. Li, Z. Li and J. Zhang, Enhanced photocatalytic hydrogen production through tuning charge transfer in TiO2/CdSxSe1–x-DETA nanocomposites with S-scheme heterojunction structure, *J. Materiomics*, 2025, **11**(3), 100919, DOI: 10.1016/j.jmat.2024.06.010.

26 X. Liu, *et al.*, Type II/Schottky heterojunctions-triggered multi-channels charge transfer in Pd-TiO2-Cu2O hybrid promotes photocatalytic hydrogen production, *J. Colloid Interface Sci.*, 2025, **685**, 173–185, DOI: 10.1016/j.jcis.2025.01.091.

27 Z. Yang, *et al.*, Improving Glycerol Photoreforming Hydrogen Production Over Ag2O-TiO2 Catalysts by Enhanced Colloidal Dispersion Stability, *Front. Chem.*, 2020, **11**(3), 100919, DOI: 10.3389/fchem.2020.00342.

28 M. M. Sarafraz and F. C. Christo, Visible light-driven photothermal Au/Ag/TiO2 trihybrid plasmonic nanomaterial for synthetic fuel production, *Int. J. Hydrogen Energy*, 2022, **47**(60), 25130–25144, DOI: 10.1016/j.ijhydene.2022.05.261.

29 Y. Zhang, *et al.*, Surface plasmon resonance metal-coupled biomass carbon modified TiO2 nanorods for photoelectrochemical water splitting, *Chin. J. Chem. Eng.*, 2022, **41**, 403–411, DOI: 10.1016/j.cjche.2021.10.022.

30 H. Pan, J. Li, Y. Wang, Q. Xia, L. Qiu and B. Zhou, Solar-Driven Biomass Reforming for Hydrogen Generation: Principles, Advances, and Challenges, *Adv. Sci.*, 2024, **11**(29), 2402651, DOI: 10.1002/advs.202402651.

31 S. Belda, *et al.*, Production of H2 and organic acids by cellulose photo-reforming with TiO2-bimetallic(CuNi) co-catalysts: Metal loading and photodeposition sequence effects, *Environ. Res.*, 2025, **271**, 121141, DOI: 10.1016/j.envres.2025.121141.

32 M. C. Herrera-Beurnio, *et al.*, Glycerol photoreforming for photocatalytic hydrogen production on binary and ternary Pt-g-C3N4-TiO2 systems: A comparative study, *Catal. Today*, 2024, **430**, 114548, DOI: 10.1016/j.cattod.2024.114548.

33 A. Y. Zerga, M. Tahir, H. Alias and A. R. Mohamed, Sludge-derived biochar nanotexture to construct BC/TiO2 composite with metallic elements influential effect for efficient photocatalytic hydrogen evolution, *Fuel*, 2024, **369**, 131678, DOI: 10.1016/j.fuel.2024.131678.

34 A. Abraham, *et al.*, Synthesis of Pd-Integrated Carbon Dot@TiO2 Thin Film for Photocatalytic Glycerol Reforming Reaction for Producing Hydrogen, *Chem. – Asian J.*, 2025, **20**(22), e00757, DOI: 10.1002/asia.202500757.

35 P. Özdemir and R. Yıldırım, Photocatalytic glycerol reforming on Pt, Au and Cu supported by reduced TiO2 under visible light irradiation, *Int. J. Hydrogen Energy*, 2024, **52**, 283–294, DOI: 10.1016/j.ijhydene.2023.05.089.

36 T. Seadira, T. Nelushi, G. Sadanandam and M. Scurrell, Photocatalytic hydrogen production from butanol reforming using Ag2O/TiO2 composite catalysts: Effects of AgxO and TiO2 precursors on the activity of the composite catalysts, *Appl. Catal. O: Open*, 2024, 206927, DOI: 10.1016/j.apcato.2024.206927.

37 U. W. Hartley, S. Amornraksa, P. Kim-Lohsoontorn and N. Laosiripojana, Thermodynamic analysis and experimental study of hydrogen production from oxidative reforming of n-butanol, *Chem. Eng. J.*, 2015, **278**, 2–12, DOI: 10.1016/j.cej.2015.02.016.

38 L. Huang, J. Zhou, A. T. Hsu and R. Chen, Catalytic partial oxidation of n-butanol for hydrogen production over LDH-derived Ni-based catalysts, *Int. J. Hydrogen Energy*, 2013, **38**(34), 14550–14558, DOI: 10.1016/j.ijhydene.2013.09.068.

39 J. Talat-Mehrabad, M. Khosravi, N. Modirshahla and M. A. Behnajady, Sol-gel preparation and characterization of Ag and Mg co-doped nano TiO2: Efficient photocatalytic degradation of C.I. Acid Red 27, *Res. Chem. Intermed.*, 2016, **42**(2), 595–609, DOI: 10.1007/s11164-015-2044-z.

40 T. W. P. Seadira, C. M. Masuku and M. S. Scurrell, Solar photocatalytic glycerol reforming for hydrogen production over Ternary Cu/THS/graphene photocatalyst: Effect of Cu and graphene loading, *Renewable Energy*, 2020, **156**, 84–97, DOI: 10.1016/j.renene.2020.04.020.

41 M. N. Chong, B. Jin, C. W. K. Chow and C. Saint, Recent developments in photocatalytic water treatment technology: A review, *Water Res.*, 2010, **44**(10), 2997–3027, DOI: 10.1016/j.watres.2010.02.039.

42 M. Thommes, *et al.*, Physisorption of gases, with special reference to the evaluation of surface area and pore size distribution (IUPAC Technical Report), *Pure Appl. Chem.*, 2015, **87**(9–10), 1051–1069, DOI: 10.1515/pac-2014-1117.

43 J. Yu, G. Wang, B. Cheng and M. Zhou, Effects of hydrothermal temperature and time on the photocatalytic activity and microstructures of bimodal mesoporous TiO2 powders, *Appl. Catal., B*, 2007, **69**(3–4), 171–180, DOI: 10.1016/j.apcatb.2006.06.022.

44 X. Chen and S. S. Mao, Titanium dioxide nanomaterials: Synthesis, properties, modifications and applications, *Chem. Rev.*, 2007, **107**(7), 2891–2959, DOI: 10.1021/cr0500535.

45 J. K. Reddy, K. Lalitha, P. V. L. Reddy, G. Sadanandam, M. Subrahmanyam and V. D. Kumari, Fe/TiO2: A visible light active photocatalyst for the continuous production of hydrogen from water splitting under solar irradiation, *Catal. Lett.*, 2014, **144**(2), 340–346, DOI: 10.1007/s10562-013-1112-5.

46 J. Yu, J. Xiong, B. Cheng and S. Liu, Fabrication and characterization of Ag-TiO2 multiphase nanocomposite thin films with enhanced photocatalytic activity, *Appl. Catal., B*, 2005, **60**(3–4), 211–221, DOI: 10.1016/j.apcatb.2005.03.009.

47 J. G. Kang and Y. Sohn, Interfacial nature of Ag nanoparticles supported on TiO 2 photocatalysts, *J. Mater. Sci.*, 2012, **47**(2), 824–832, DOI: 10.1007/s10853-011-5860-6.

48 T. W. P. Seadira, G. Sadanandam, T. Ntho, C. M. Masuku and M. S. Scurrell, Preparation and characterization of metals supported on nanostructured TiO2 hollow spheres for production of hydrogen via photocatalytic reforming of glycerol, *Appl. Catal., A*, 2018, **222**, 133–145, DOI: 10.1016/j.apcatb.2017.09.072.

49 G. Sadanandam, K. Lalitha, V. D. Kumari, M. V. Shankar and M. Subrahmanyam, Cobalt doped TiO2: A stable and efficient photocatalyst for continuous hydrogen production from glycerol: Water mixtures under solar light irradiation, *Int. J. Hydrogen Energy*, 2013, **38**(23), 9655–9664, DOI: 10.1016/j.ijhydene.2013.05.116.

50 R. A. Rather, S. Singh and B. Pal, Visible and direct sunlight induced H2 production from water by plasmonic Ag-TiO2 nanorods hybrid interface, *Sol. Energy Mater. Sol. Cells*, 2017, **160**, 463–469, DOI: 10.1016/j.solmat.2016.11.017.

51 K. Selvam, M. Muruganandham, I. Muthuvel and M. Swaminathan, The influence of inorganic oxidants and metal ions on semiconductor sensitized photodegradation of 4-fluorophenol, *Chem. Eng. J.*, 2007, **128**(1), 51–57, DOI: 10.1016/j.cej.2006.07.016.

52 T. Sugimoto, X. Zhou and A. Muramatsu, Synthesis of uniform anatase TiO2 nanoparticles by gel-sol method: 3. Formation process and size control, *J. Colloid Interface Sci.*, 2003, **259**(1), 43–52, DOI: 10.1016/S0021-9797(03)00036-5.

53 D. Jing, M. Liu, J. Shi, W. Tang and L. Guo, Hydrogen production under visible light by photocatalytic reforming of glucose over an oxide solid solution photocatalyst, *Catal. Commun.*, 2010, **12**(4), 264–267, DOI: 10.1016/j.catcom.2010.09.031.

54 T. W. P. Seadira, S. J. Baloyi, C. M. Masuku and M. S. Scurrell, Solar photocatalytic hydrogen production from glycerol reforming using ternary Cu/THS/Graphene, in *IOP Conference Series: Materials Science and Engineering*, Institute of Physics Publishing, Nov. 2019, DOI: 10.1088/1757-899X/655/1/012049.

55 N. Strataki, V. Bekiari, D. I. Kondarides and P. Lianos, Hydrogen production by photocatalytic alcohol reforming employing highly efficient nanocrystalline titania films, *Appl. Catal., B*, 2007, **77**(1–2), 184–189, DOI: 10.1016/j.apcatb.2007.07.015.

56 W. Cui, L. Feng, C. Xu, S. Lü and F. Qiu, Hydrogen production by photocatalytic decomposition of methanol gas on Pt/TiO2 nano-film, *Catal. Commun.*, 2004, **5**(9), 533–536, DOI: 10.1016/j.catcom.2004.06.011.